Nonmagnetic ground state in the cubic compounds $PrNi_2Cd_{20}$ and $PrPd_2Cd_{20}$

D. Yazici,[1,2] T. Yanagisawa,[3] B. D. White,[1,2] and M. B. Maple[1,2,*]

[1]*Department of Physics, University of California, San Diego, La Jolla, California 92093, USA*

[2]*Center for Advanced Nanoscience, University of California, San Diego, La Jolla, California 92093, USA*

[3]*Department of Physics, Hokkaido University, Sapporo 060-0810, Japan*

(Received 20 November 2014; revised manuscript received 24 February 2015; published 23 March 2015)

Temperature-dependent magnetization, specific-heat, and electrical-resistivity measurements were performed on single crystals of $PrNi_2Cd_{20}$ and $PrPd_2Cd_{20}$. Neither compound shows any evidence for magnetic order above 2 K. Magnetization measurements suggest that Pr ions assume a nonmagnetic Γ_1 singlet or non-Kramers Γ_3 doublet ground state. A broad peak, which is identified as a Schottky anomaly, is observed in the specific heat at low temperature. Low-lying excitations involving the $4f$ electrons persist down to 2 K for both $PrNi_2Cd_{20}$ and $PrPd_2Cd_{20}$ and related features are also observed in the magnetization and electrical resistivity.

DOI: 10.1103/PhysRevB.91.115136 PACS number(s): 71.27.+a, 72.15.Eb, 75.30.Mb, 75.40.Cx

I. INTRODUCTION

Exotic physical properties originating from strong electronic correlations in Pr-based cubic compounds have attracted much attention. In these systems, if the crystalline electric field (CEF) ground state of the Hund's rule $J = 4$ multiplet is a nonmagnetic, non-Kramers doublet (Γ_3), the fluctuating quadrupolar moment can interact with the conduction electrons to produce strongly correlated behavior [1]. Intriguing phenomena such as multipolar ordering and the multipolar Kondo effect are expected to occur in such a scenario [1]. The pseudobinary system $Y_{1-x}U_xPd_3$ is the first example of non-Fermi-liquid (NFL) behavior in an f-electron system; its behavior was originally interpreted in terms of a quadrupolar Kondo effect [2–4], which is a version of a spin 1/2 two-channel Kondo effect. The quadrupolar Kondo effect requires that nearly localized tetravalent uranium ions in a cubic local environment with CEF-split $5f$ energy levels are covalently admixed with conduction band electron states, generating an antiferromagnetic exchange interaction which leads to the Kondo effect [2–4]. In the Russell-Saunders coupling scheme, U^{4+} has the same series of CEF levels as Pr^{3+}, indicating that similar behavior can be observed in Pr-based compounds [5]. Another prominent example of quadrupolar phenomena is antiferroquadrupolar (AFQ) order arising from the doublet ground state in $PrPb_3$ [6,7], in which chemical substitution of La for Pr destroys the AFQ order at $x = 0.03$ in $Pr_{1-x}La_xPb_3$ [8]. NFL behavior in this system, observed in the specific heat for $x \geqslant 0.95$, was attributed to the quadrupolar Kondo effect [8]. On the other hand, if the ground state is a nonmagnetic singlet (Γ_1), superconductivity may be mediated by quadrupolar fluctuations as apparently occurs in the Pr-based heavy-fermion superconductor $PrOs_4Sb_{12}$, which has a superconducting transition temperature $T_c = 1.86$ K [9–16].

The Pr-based compounds PrM_2X_{20} (M = Ti, V, Nb, Ru, Rh, Ir; X = Al, Zn) with a cubic $CeCr_2Al_{20}$-type crystal structure have attracted much interest [17–25]. In a cubic CEF, the $J = 4$ multiplet of the Pr^{3+} ion splits into four levels: a Γ_1 singlet, a Γ_3 non-Kramers doublet, and Γ_4 and Γ_5 triplets. One of the important features of the PrM_2X_{20} compounds is that, in most cases, the Γ_3 doublet is considered to be the ground state [18,21,22,25]. Indeed, a recent inelastic neutron scattering study [23] and ultrasonic velocity measurements [26] have confirmed that the Γ_3 doublet is the ground state in $PrTi_2Al_{20}$ and $PrIr_2Zn_{20}$. Recently, we succeeded in synthesizing RM_2Cd_{20} (R = rare earth; M = Ni, Pd) compounds in single-crystalline form [27]. Systematic studies of the structural, magnetic, electrical transport, and thermodynamic properties of the RM_2Cd_{20} family were recently published [27,28]. Since all of the known PrM_2X_{20} (X = Al, Zn) compounds are heavy-fermion materials [17–25], we were motivated to study these X = Cd compounds to ascertain whether they also exhibit strong electronic correlations or multipolar order.

In this paper, we report dc magnetization M, electrical-resistivity ρ, and specific-heat C measurements on single-crystalline samples of PrM_2Cd_{20} (M = Ni, Pd) and a reference compound $LaNi_2Cd_{20}$. The monotonic increase of M with H and a Van Vleck–type behavior at low temperatures in M/H versus T data indicate that the ground state of Pr in $PrNi_2Cd_{20}$ and $PrPd_2Cd_{20}$ is a non-Kramers Γ_3 doublet or Γ_1 singlet. The $C(T)$ data exhibit a broad peak which resembles a Schottky anomaly and the $\rho(T)$ data display a nearly linear dependence on T below $T \sim 11$ K; these features are related to the low-lying excitations involving the $4f$ electrons in both $PrNi_2Cd_{20}$ and $PrPd_2Cd_{20}$.

II. EXPERIMENTAL DETAILS

Single crystals of PrM_2Cd_{20} (M = Ni, Pd) and $LaNi_2Cd_{20}$ were prepared by the Cd self-flux method. Details of the sample preparation are described in Ref. [27]. Crystal structure and sample quality were primarily characterized through analysis of powder x-ray diffraction (XRD) patterns collected with a Bruker D8 Discover x-ray diffractometer. Four-wire electrical-resistivity measurements were performed from 300 K down to ~1.1 K in a pumped ^{4}He Dewar. Magnetization measurements were performed between 300 and 2 K in a Quantum Design Magnetic Property Measurement System (MPMS). Specific-heat measurements were performed down to 1.8 K using a Physical Property Measurement System (PPMS) DynaCool. The specific-heat measurements were made using a standard thermal relaxation technique.

*Corresponding author: mbmaple@ucsd.edu

TABLE I. Summary of structural, magnetic, electrical transport, and thermodynamic data for PrM_2Cd_{20} (M = Ni, Pd) compounds. Listed are the cubic lattice parameter a; Curie-Weiss temperature Θ_{CW}; effective magnetic moment μ_{eff}; residual resistivity ρ_0, measured at $T \sim 1.2$ K; residual resistance ratio RRR $\equiv R(300\text{ K})/R(1.2\text{ K})$; and linear coefficient of the specific heat γ.

Compound	a (Å)	Θ_{CW} (K)	μ_{eff} (μ_B)	ρ_0 ($\mu\Omega$ cm)	RRR	γ $\left(\frac{\text{mJ}}{\text{mol}-\text{K}^2}\right)$
$PrNi_2Cd_{20}$	15.575(1)	−0.4	3.51	0.64	21	14
$PrPd_2Cd_{20}$	15.699(1)	−3.2	3.60	0.57	29	250

The orientation of single crystals was determined using a Bruker D8 Discover x-ray diffractometer.

III. RESULTS AND DISCUSSION

Analysis of the powder XRD patterns indicated that the PrM_2Cd_{20} (M = Ni, Pd) and $LaNi_2Cd_{20}$ samples are single phase without any trace of impurity phases. The lattice parameter from the Rietveld refinements, which were conducted on powder XRD patterns for each sample using GSAS [29] and EXPGUI [30], are given in Table I. The $CeCr_2Al_{20}$-type cubic crystal structure with space group $Fd\bar{3}m$ was observed for all samples [27]. XRD patterns for the PrM_2Cd_{20} (M = Ni, Pd) and $LaNi_2Cd_{20}$ single crystals are shown in Fig. 1, plotted with their refined patterns for comparison. This crystal structure provides an opportunity to study strongly correlated electronic states, which can be associated with either f or d electrons, and localized Pr magnetic moments that have a large spatial separation [27,28]. The larger spatial separation between Pr ions of 6.74 and 6.80 Å for $PrNi_2Cd_{20}$ and $PrPd_2Cd_{20}$, respectively, relative to that in Pr-based 1-2-20 compounds

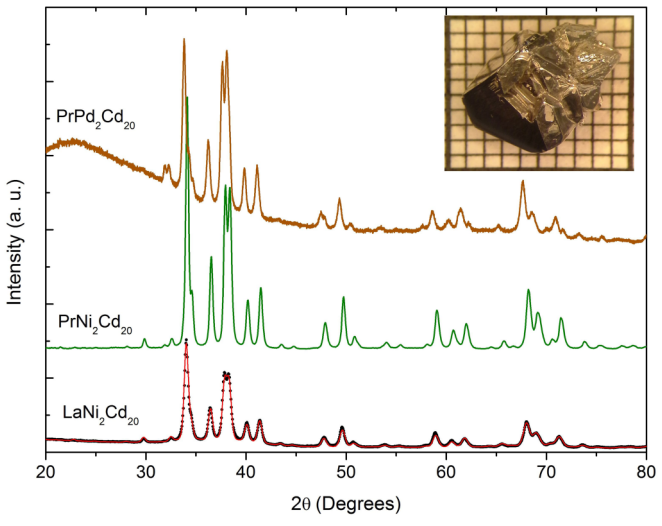

FIG. 1. (Color online) X-ray diffraction patterns for $PrNi_2Cd_{20}$, $PrPd_2Cd_{20}$, and $LaNi_2Cd_{20}$ measured at room temperature. The black circles and green and brown lines indicate the observed intensity I_{obs} for $LaNi_2Cd_{20}$, $PrNi_2Cd_{20}$, and $PrPd_2Cd_{20}$, respectively. The red line represents the calculated intensity I_{calc}. A photograph of a $PrNi_2Cd_{20}$ single crystal is shown in the inset where the small squares are 1 mm × 1 mm for reference.

based on Zn and Al [21,31], would be expected to result in weaker hybridization between localized $4f$ and itinerant electron states and smaller magnetic exchange interaction strength in $PrNi_2Cd_{20}$ and $PrPd_2Cd_{20}$.

Magnetization divided by magnetic field M/H data are displayed as a function of temperature in Fig. 2(a). Measurements were performed in magnetic fields $\mu_0 H = 0.1$ T for $PrNi_2Cd_{20}$, $\mu_0 H = 1$ T for $PrPd_2Cd_{20}$, and $\mu_0 H = 5$ T for $LaNi_2Cd_{20}$, with H applied parallel to the ⟨111⟩ direction, between 2 and 300 K. The $PrNi_2Cd_{20}$ and $PrPd_2Cd_{20}$ compounds exhibit a Curie-Weiss–type $M(T)/H$ behavior with no noticeable anomalies indicative of any magnetic order down to 2 K. M is a linear function of H in Fig. 2(b) up to these magnetic field values, so it follows that $M/H \approx \chi$ where $\chi(T)$ is the magnetic susceptibility. The χ^{-1} versus T data for $PrNi_2Cd_{20}$ and $PrPd_2Cd_{20}$ were fitted using a Curie-Weiss law

$$\chi - \chi_0 = \frac{C_0}{(T - \Theta_{CW})}, \tag{1}$$

in the temperature range ∼20–300 K to determine the Curie-Weiss temperature Θ_{CW} and effective magnetic moment μ_{eff} of Pr. We extracted μ_{eff} from the Curie constant $C_0 = N_A\mu_{eff}^2/3k_B$, where N_A is Avogadro's number and k_B is Boltzmann's constant. The fits of Eq. (1) to the data were performed using a nonlinear least-squares regression. The resulting best-fit parameter values for μ_{eff} and Θ_{CW} are tabulated in Table I. The theoretical Pr^{3+} free-ion magnetic moment is $\mu_{eff} = g_J[J(J+1)]^{1/2}\mu_B = 3.58\ \mu_B$/Pr, where $g_J = 0.8$ is the Landé g factor and $J = 4$. The values $\mu_{eff} = 3.51$ and 3.60 μ_B/f.u., obtained from the fits of Eq. (1) to the $\chi(T)$ data for $PrNi_2Cd_{20}$ and $PrPd_2Cd_{20}$, respectively, are close to the theoretical Pr^{3+} free-ion value which indicates that the $4f$ electrons are well localized in these compounds. The negative values of Θ_{CW}, −0.4 K for $PrPd_2Cd_{20}$ and −3.2 K for $PrPd_2Cd_{20}$, reflect the weak antiferromagnetic interactions in these compounds involving the first excited triplet CEF level. Below ∼15 K, the dc magnetization deviates from the Curie-Weiss fit and saturates towards a value of ∼0.26 emu/mol-Oe as $T \to 0$ K for both $PrNi_2Cd_{20}$ and $PrPd_2Cd_{20}$, as shown in Fig. 2(c). This behavior indicates that the ground state of the Pr^{3+} ions is nonmagnetic (Γ_1 or Γ_3) with a low-lying triplet excited state separated from the ground state.

The M versus H data, measured at 2 K with H parallel to the ⟨111⟩ direction for $PrNi_2Cd_{20}$ and $PrPd_2Cd_{20}$, are displayed in Fig. 2(b). The magnetization increases monotonically with H up to 5 T without exhibiting any anomalies or saturating. This is consistent with a nonmagnetic Γ_1 singlet or a non-Kramers Γ_3 doublet ground state. The $M(H)$ isotherms at high temperatures are approximately linear for both $PrNi_2Cd_{20}$ and $PrPd_2Cd_{20}$, as illustrated by the M versus H data measured at 50 K for $PrPd_2Cd_{20}$ with H parallel to the ⟨111⟩ direction [see Fig. 2(c)].

No anomalies associated with superconductivity or magnetic order were observed throughout the temperature range of the measurements. The lack of magnetic order above 2 K as well as the monotonic increase of M with H for both $PrNi_2Cd_{20}$ and $PrPd_2Cd_{20}$ indicate that the Pr^{3+} ions have a nonmagnetic ground state. The ninefold-degenerate Pr^{3+} $J = 4$ Hund's rule multiplet splits in a cubic CEF into a

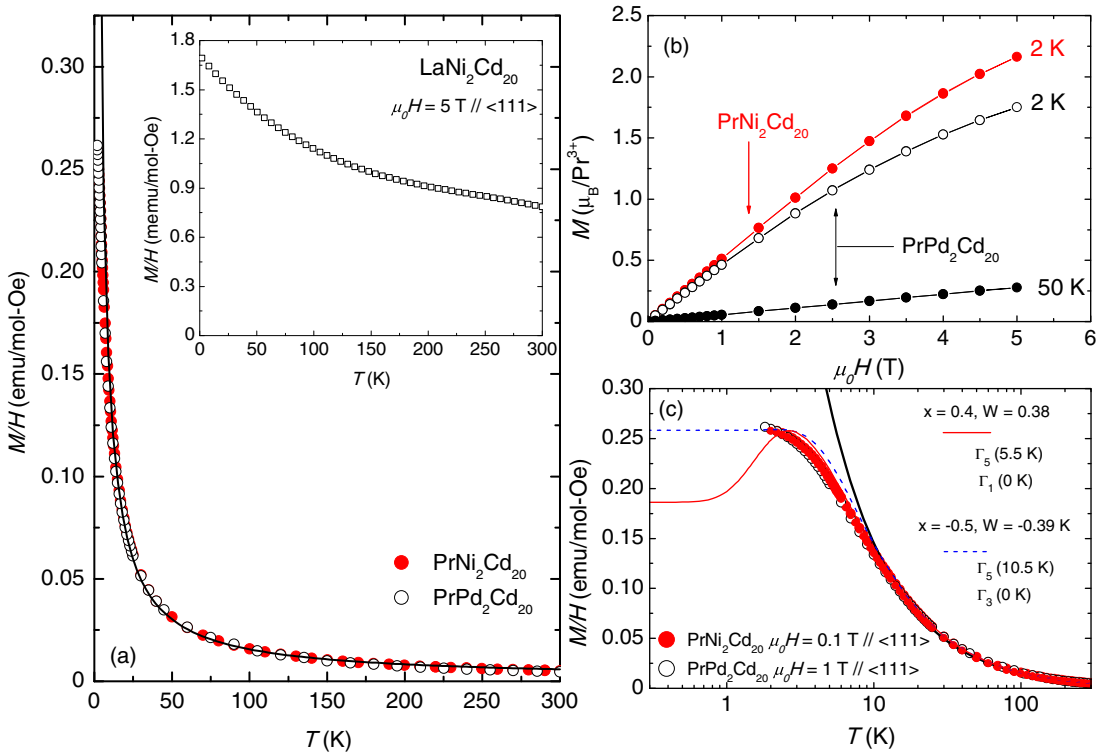

FIG. 2. (Color online) (a) Magnetic susceptibility M/H as a function of temperature T, measured in magnetic fields $\mu_0 H = 0.1$ T for $PrNi_2Cd_{20}$ and $\mu_0 H = 1$ T for $PrPd_2Cd_{20}$. The solid line represents a Curie-Weiss law, fitted to the data above 20 K. Inset: M/H versus T data for $LaNi_2Cd_{20}$, measured in a magnetic field $\mu_0 H = 5$ T. (b) M versus $\mu_0 H$ data with H applied parallel to the $\langle 111 \rangle$ direction for $PrNi_2Cd_{20}$ and $PrPd_2Cd_{20}$ at $T = 2$ K and for $PrPd_2Cd_{20}$ at $T = 50$ K. (c) Plot of M/H versus $\ln T$ for $PrNi_2Cd_{20}$ and $PrPd_2Cd_{20}$ below 300 K. The solid red and dashed blue lines are fits of M/H versus T for $PrNi_2Cd_{20}$ based on a CEF model with Pr^{3+} Γ_1 singlet and Γ_3 doublet ground states, respectively. The solid black line represents a Curie-Weiss law fit. See the text for an explanation of the parameters.

Γ_1 singlet, a Γ_3 doublet, and Γ_4 and Γ_5 triplet states. Given a nonmagnetic ground state, CEF fits to the M/H versus T data [see Fig. 2(b)] were performed for the cases of both Γ_1 singlet and Γ_3 doublet ground states for $PrNi_2Cd_{20}$ (after the M/H versus T data for $LaNi_2Cd_{20}$ were subtracted) and $PrPd_2Cd_{20}$ (not shown here) [5]. The CEF parameters $x_{\rm LLW}$ and W, used to make the fits, are from Lea, Leask, and Wolf (LLW), where $x_{\rm LLW}$ is the ratio of the fourth- and sixth-order terms of the angular momentum operators in the crystal field Hamiltonian and W is an overall energy scale [5]. The best fit for $PrNi_2Cd_{20}$ and $PrPd_2Cd_{20}$ with a Γ_1 singlet ground state was found for $x_{\rm LLW} = 0.4$ and $W = 0.38$, which results in an energy-level splitting of 5.5 K between the Γ_1 singlet ground state and the Γ_5 triplet first excited state in zero magnetic field. The low-temperature behavior of the M/H data is not accurately reproduced by the CEF fit, similar to the case of $PrOs_4Sb_{12}$, which was determined to have a nonmagnetic Γ_1 singlet ground state [9]. For the case of a nonmagnetic Γ_3 doublet ground state, the best fit was found for $x_{\rm LLW} = -0.5$ and $W = -0.39$, resulting in an energy splitting of 10.5 K between the Γ_3 ground state and the Γ_5 first excited state in zero magnetic field. The M/H data could also be fitted with parameters $x_{\rm LLW} = -0.4$ and $W = -0.3$, resulting in an energy-level splitting of 11.5 K between the Γ_3 ground state and the Γ_5 first excited state in zero magnetic field. However, the latter scenario is unlikely because the parameters $x_{\rm LLW} = -0.4$ and $W = -0.3$ are at the point where the Γ_4 and Γ_5 excited states are nearly degenerate, which requires a large entropy according to theoretical calculations [5]. However, the total entropy S_T attains a value of only $\sim$9.87 and $\sim$10.5 J mol^{-1} K^{-1} for $PrNi_2Cd_{20}$ and $PrPd_2Cd_{20}$, respectively (discussed later).

Electrical resistivity ρ versus temperature T data in zero magnetic field for the compounds $PrNi_2Cd_{20}$, $PrPd_2Cd_{20}$, and $LaNi_2Cd_{20}$ are displayed in Fig. 3. The current flows in the the $\langle 111 \rangle$ direction. Metallic behavior is observed for each compound with no indication of a coherence peak. The zero-field residual resistance ratios RRR $\equiv R(300\ {\rm K})/R(1.2\ {\rm K})$ for $PrNi_2Cd_{20}$ and $PrPd_2Cd_{20}$ were found to be $\sim$20 and $\sim$29, respectively, which indicates that the single crystals are of high quality. The electrical resistivity decreases down to 2 K without any other anomalies indicative of phase transitions, consistent with a nonmagnetic CEF ground state. Electrical resistivity ρ versus T data below 50 K for $PrNi_2Cd_{20}$, $PrPd_2Cd_{20}$, and $LaNi_2Cd_{20}$ are displayed in the inset of Fig. 3(a) to highlight the nearly linear T dependence of ρ at low temperatures below $\sim$20 K. The red solid lines in the inset of Fig. 3(a) are guides to the eye showing the change in $\partial\rho/\partial T$ for $PrPd_2Cd_{20}$.

An exemplary log-log plot of the temperature dependence of $\rho - \rho_0$ versus T below 50 K for $PrNi_2Cd_{20}$, where ρ_0 is the residual resistivity, is presented in Fig. 3(b). In order to analyze the behavior of the electrical resistivity, the $\rho(T) - \rho_0$ data were fitted with a power law of the form $\rho - \rho_0 = BT^n$. The

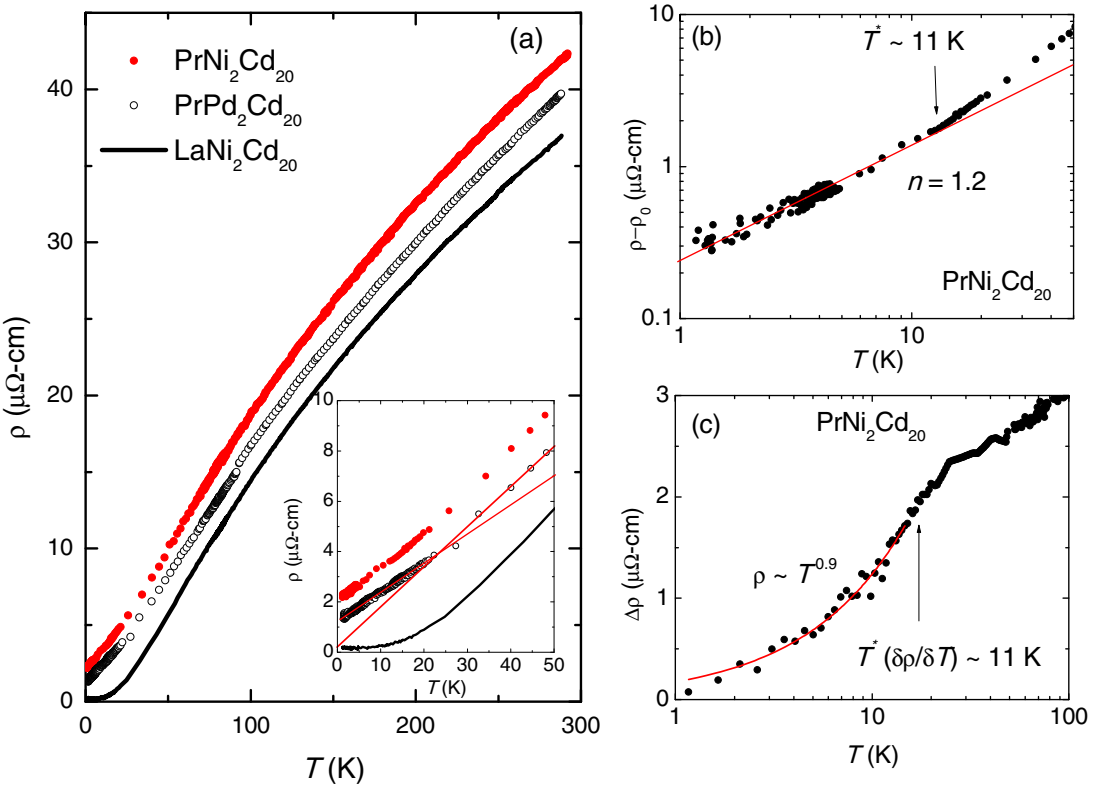

FIG. 3. (Color online) (a) Electrical resistivity ρ versus temperature T for $PrNi_2Cd_{20}$, $PrPd_2Cd_{20}$, and $LaNi_2Cd_{20}$. Inset: Low-T ρ versus T for $PrNi_2Cd_{20}$, $PrPd_2Cd_{20}$, and $LaNi_2Cd_{20}$. The red solid lines are guides to the eye marking a change in $\partial\rho/\partial T$ for $PrPd_2Cd_{20}$. (b) ρ-ρ_0 versus T on a log-log plot together with a power-law fit (red solid line) for $PrNi_2Cd_{20}$. The fit extends to a temperature $T^* \simeq 11$ K. (c) Temperature dependence of the incremental electrical resistivity $\Delta\rho(T) = \rho(T) - \rho_{\rm lat}(T) - \rho_0$ versus T on a semi-log plot together with a power-law fit (red solid line) for $PrNi_2Cd_{20}$ (described in the text).

best-fit parameter values for ρ_0 are listed in Table I. The values of the exponent n for both $PrNi_2Cd_{20}$ and $PrPd_2Cd_{20}$ below $\sim$11K are $n \simeq 1.2$, indicating that each could exhibit NFL ($n < 2$) behavior [32,33]. To further evaluate the contribution to the electrical resistivity due to scattering from localized $4f$ electron states in $PrNi_2Cd_{20}$, $\Delta\rho(T)$ [sometimes expressed as $\rho_{4f}(T)$] the electron-phonon scattering component has been subtracted using $\rho(T)$ data for the $LaNi_2Cd_{20}$ reference compound which does not contain $4f$ electrons. A shoulderlike feature near $T \sim 11$ K in the zero-field $\rho(T)$ curve for $PrNi_2Cd_{20}$ reflects the reduction in scattering of conduction electrons by the Pr ions due to the depopulation of the excited-state triplet with decreasing temperature. This feature is consistent with the temperature where M/H starts to deviate from Curie-Weiss behavior. Since we were unable to synthesize a reference compound for $PrPd_2Cd_{20}$, we could not analyze the change in $\partial\rho/\partial T$ below 20 K for this compound.

Plots of C/T versus T for $PrNi_2Cd_{20}$, $PrPd_2Cd_{20}$, and $LaNi_2Cd_{20}$ are shown in Fig. 4(a). A Schottky-type peak in the specific-heat data of $PrNi_2Cd_{20}$ and $PrPd_2Cd_{20}$ is visible below $\sim$20 and $\sim$15 K, respectively. In order to analyze the conduction electron and $4f$ electron contribution to the specific heat for $PrNi_2Cd_{20}$ in zero magnetic field, $\Delta C(T)/T = [\gamma + C_{4f}(T)]/T$, we subtracted the phonon contribution, estimated from $C(T)/T$ data for $LaNi_2Cd_{20}$, from $C(T)/T$ data for $PrNi_2Cd_{20}$. The result is shown in Fig. 4(b). The similar slopes of the data for $T \geqslant 30$ K indicate that the lattice contribution for $PrPd_2Cd_{20}$ is comparable to that of the nonmagnetic reference compound $LaNi_2Cd_{20}$. Therefore, the $C(T)$ data for $LaNi_2Cd_{20}$ were scaled by a factor of 1.02 to account for slight differences in Θ_D. The resultant $\Delta C(T)/T$ data for $PrPd_2Cd_{20}$, after subtracting the phonon and conduction electron contributions, are shown in Fig. 4(c). Further evidence for a splitting $\delta \sim 10-15$ K between the Pr^{3+} Γ_1 or Γ_3 nonmagnetic ground state and Γ_5 triplet first excited state was derived from a fit of the Schottky-type anomaly in the $\Delta C(T)/T$ data for $PrNi_2Cd_{20}$ and $PrPd_2Cd_{20}$. The Schottky-type anomaly, centered around 4 K for $PrNi_2Cd_{20}$ [Fig. 4(b)] and 3 K for $PrPd_2Cd_{20}$ [Fig. 4(c)], was fitted from 1.8 to 30 K and 1.8 to 20 K for $PrNi_2Cd_{20}$ and $PrPd_2Cd_{20}$, respectively, using the equation $\Delta C(T)/T = \gamma + AC_{\rm Sch}(T)/T$. Here, $C_{\rm Sch}(T) = (\delta/T)^2(g_a/g_b)\exp(-\delta/T)[1 + (g_a/g_b)\exp(-\delta/T)]^{-2}$, where g_a (g_b) is the degeneracy of the ground state (first excited state), δ is the energy-level splitting, and A is a scale factor. Any nuclear contribution was assumed to be negligible in this temperature range. The best fits for $PrNi_2Cd_{20}$ are shown in Fig. 4(b) for a Γ_1 singlet ground state and a Γ_5 triplet first excited state scaled by $A = 0.4$ (blue dashed line) with a splitting $\delta \approx 5.5$ K, and for a Γ_3 doublet ground state and a Γ_5 triplet first excited state scaled by $A = 0.9$ (red solid line) with $\delta = 12$ K and an additional electronic contribution $\gamma \approx 14$ mJ/mol $-$ K^2.

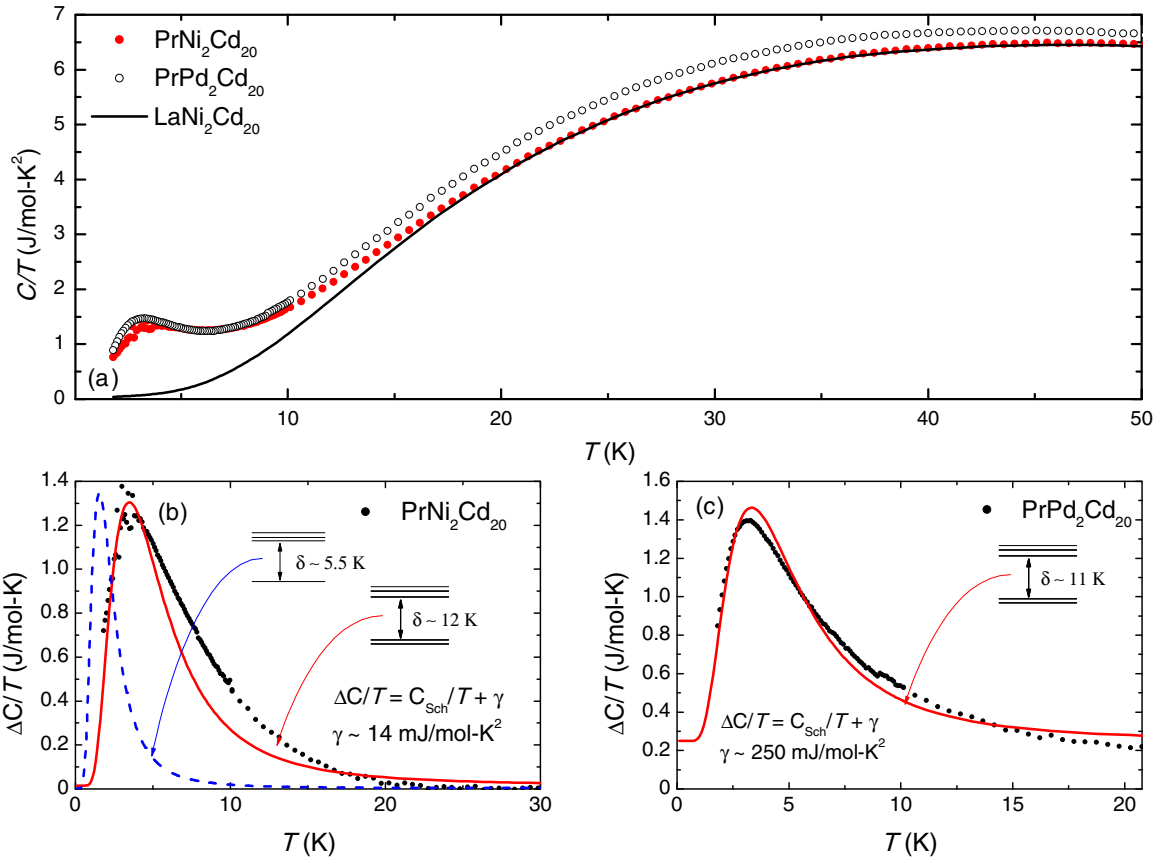

FIG. 4. (Color online) (a) Specific heat divided by temperature C/T versus temperature T for $PrNi_2Cd_{20}$, $LaNi_2Cd_{20}$, and $PrPd_2Cd_{20}$ in zero magnetic field. (b) $4f$ electron contribution to the specific heat divided by temperature $\Delta C/T$ versus T for $PrNi_2Cd_{20}$ (see text for details). The dashed blue line is a fit to a two-level Schottky anomaly, scaled by a factor of 0.4, assuming a Pr^{3+} Γ_1 ground state. The solid blue line is a fit to a two-level Schottky anomaly, scaled by 0.9, assuming a Pr^{3+} Γ_3 ground state. The level splittings δ were taken from our fits of M/H data. (c) $4f$ electron contribution to the specific heat divided by temperature $\Delta C/T$ versus T for $PrPd_2Cd_{20}$ (see text for details). The solid red line is a fit to a two-level Schottky anomaly and an electronic term γ assuming a Pr^{3+} Γ_3 ground state (see text for details).

The scaling of the Schottky anomaly required to achieve an accurate fit for a Γ_3 doublet ground state ($A = 0.9$) could be a result of significant hybridization of the localized $4f$ and itinerant electron states. Such a transfer of entropy from the localized $4f$ electrons to the conduction electrons has been observed previously in the heavy-fermion superconductor $PrOs_4Sb_{12}$ [10]. One can see that the Γ_1 ground-state fit to the $\Delta C(T)/T$ data is not suitable using a similar δ value determined from CEF fitting of the M/H versus T data. We were able to obtain a better fit by allowing δ to vary, but the resulting value is inconsistent with the analysis of the M/H versus T data; this may be an indication that the ground-state Γ_3 CEF scheme is more appropriate. However, since this low-lying excitation is spread out in a wide temperature range below 20 K for $PrNi_2Cd_{20}$ and $PrPd_2Cd_{20}$, it is difficult to describe the Schottky-type anomaly with a definite energy scale arising from the CEF splitting of the Pr^{3+} energy level. In order to reveal the details of the low-lying excitation, it is essential to measure the specific heat at lower temperatures.

The best fit for the Schottky anomaly in $PrPd_2Cd_{20}$ is shown in Fig. 4(c) for a Γ_3 doublet ground state and a Γ_5 triplet first excited state with $A = 1, \delta = 11$ K, and $\gamma \approx 250$ mJ/mol $-$ K^2. However, the precise values of the fit parameters g_a/g_b, δ, and A are subject to uncertainty because of the broadened nature of the Schottky-type anomaly in $C(T)/T$ for both $PrNi_2Cd_{20}$ and $PrPd_2Cd_{20}$. This might be related to broken cubic symmetry, lattice instability, or site disorder. It is very likely that a small amount of Pr or Cd ions may occupy some of the Ni or Pd sites [27]. In order to confirm the proposed CEF splitting scenario, further experiments, such as low-temperature $C(T)$ measurements and inelastic neutron scattering in high applied magnetic fields, are required. However, it should be noted that Cd is a strong neutron absorber; therefore, a sample would need to be synthesized using one of the less-absorbing Cd isotopes like ^{114}Cd to conduct neutron scattering measurements [34].

The $4f$ electron contribution to the specific heat $\Delta C(T)$ (described above) of $PrNi_2Cd_{20}$ and $PrPd_2Cd_{20}$ is displayed in Figs. 5(a) and 5(b), respectively (left axis). The entropy $S = \int(\Delta C/T)dT$ (extrapolating a power-law T dependence of $\Delta C/T$ to 0 K to estimate the magnetic entropy below 1.8 K) is displayed in Figs. 5(a) and 5(b) for $PrNi_2Cd_{20}$ and $PrPd_2Cd_{20}$, respectively (right axis). $S \approx S_{4f} + S_{el}$ attains a value of $\sim$9.9 J mol^{-1} K^{-1} at 20 K for $PrNi_2Cd_{20}$ and $S \sim$ 10.5 J mol^{-1} K^{-1} for $PrPd_2Cd_{20}$ at 15 K. This latter value includes the electronic contribution $S_{el} \sim 5$ J mol^{-1} K^{-1} to the entropy. Therefore, S_{4f} reaches a value of $S_{4f} \sim$ 5.5 J mol^{-1} K^{-1} for $PrPd_2Cd_{20}$. At $\sim$6.5 and $\sim$6 K, respectively, the entropy is R ln2, implying that the

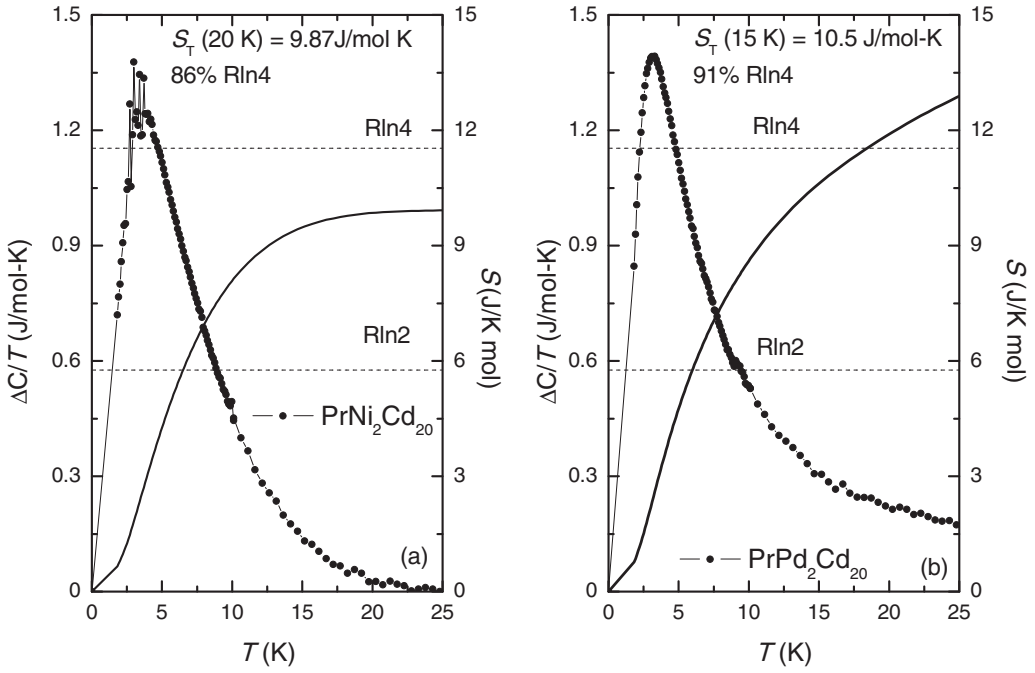

FIG. 5. (a) $\Delta\, C/T$ (left axis) versus T and the entropy S (right axis) versus T for $PrNi_2Cd_{20}$. (b) $\Delta\, C/T$ (left axis) versus T and the entropy S (right axis) versus T for $PrPd_2Cd_{20}$. S_T represents the total entropy at 20 and 15 K for $PrNi_2Cd_{20}$ and $PrPd_2Cd_{20}$, respectively.

pronounced peak in $C(T)/T$ corresponds to a Γ_3 doublet ground state; however, the possibility of a Γ_1 singlet ground state cannot be dismissed. Additionally, the presence of a fractional residual entropy of $\frac{1}{2}\,R\ln 2$, predicted for the quadrupolar Kondo model [1], might be ruled out because we observe the full degeneracy of the ground state for both $PrNi_2Cd_{20}$ and $PrPd_2Cd_{20}$.

IV. SUMMARY

Measurements of electrical resistivity, magnetization, and specific heat have been performed on single crystals of the cage compounds PrM_2Cd_{20} (M = Ni, Pd). No evidence indicating a phase transition was observed down to 1.1 K. Features observed in the temperature dependence of ρ around 11 K can be interpreted in terms of CEF splitting of the multiplet levels of the Pr^{3+} ion. The monotonic increase of M with H and Van Vleck–type behavior at low temperatures in M/H versus T data indicate a non-Kramers Γ_3 doublet or Γ_1 singlet ground state. The precise value of γ is subject to uncertainty because of experimental constraints imposed by the Schottky-type anomaly for $PrNi_2Cd_{20}$ below 20 K and for $PrPd_2Cd_{20}$ below 15 K. The large spatial Pr-Pr separation of order 6.74 and 6.80 Å for $PrNi_2Cd_{20}$ and $PrPd_2Cd_{20}$, respectively, may be the cause of the weak exchange interaction between Pr magnetic moments in $PrNi_2Cd_{20}$ and $PrPd_2Cd_{20}$. Because of the large spatial separation of Pr ions, a small electronic specific-heat coefficient for $PrNi_2Cd_{20}$ and $PrPd_2Cd_{20}$ is expected. The electrical resistivity data for $PrNi_2Cd_{20}$ and $PrPd_2Cd_{20}$ could exhibit NFL behavior below $T \sim 11$ K in which $\rho \propto T^n$ with $n \simeq 1.2$. On the other hand, the nonquadratic temperature dependence of the electrical resistivity at low temperature might reflect a reduction of the scattering of conduction electrons by the Pr ions due to the depopulation of the excited-state triplet state with decreasing temperature. A CEF modification of the low-temperature electrical resistivity by thermal depopulation of a low-lying triplet 7 K above a singlet ground state was observed in the heavy-fermion compound $PrOs_4Sb_{12}$ [35]. The specific-heat and magnetization data for $PrNi_2Cd_{20}$ and $PrPd_2Cd_{20}$ cannot be described by a logarithmic divergence or power-law behavior at low temperatures. However, such features associated with NFL behavior might be obscured by the Schottky-type anomaly for $PrNi_2Cd_{20}$ and $PrPd_2Cd_{20}$. Non-Fermi-liquid behavior was observed for the isostructural heavy-fermion compound $PrNb_2Al_{20}$ with a Γ_3 doublet ground state which is related to the quadrupole degrees of freedom [25].

Further experiments are needed to unambiguously identify the ground state of these new PrM_2Cd_{20} (M = Ni, Pd) compounds. Measurements of the magnetic field dependence of the low-temperature specific heat are in progress.

ACKNOWLEDGMENTS

Research at UCSD was supported by the US Department of Energy, Office of Basic Energy Sciences, Division of Material Sciences and Engineering under Grant No. DE-FG02-04-ER46105 (sample synthesis and physical properties measurements) and the National Science Foundation under Grant No. DMR 1206553 (low-temperature measurements). One of the authors, T. Yanasigawa, is supported by a Grant-in-Aid for Scientific Research (Grant No. 26400342) and The Strategic Young Researcher Overseas Visits Program for Accelerating Brain Circulation from the Japan Society for Promotional Science. The authors gratefully acknowledge assistance from V. W. Burnett in preparing samples.

[1] D. L. Cox, Phys. Rev. Lett. **59**, 1240 (1987).

[2] C. L. Seaman, M. B. Maple, B. W. Lee, S. Ghamaty, M. S. Torikachvili, J. S. Kang, L. Z. Liu, J. W. Allen, and D. L. Cox, J. Alloys Compd. **181**, 327 (1992).

[3] J. W. Allen, L. Z. Liu, R. O. Anderson, C. L. Seaman, M. B. Maple, Y. Dalichaouch, J.-S. Kang, M. S. Torikachvili, and M. A. Lopez de la Torre, Phys. B (Amsterdam) **186-188**, 307 (1993).

[4] L. Z. Liu, J. W. Allen, C. L. Seaman, M. B. Maple, Y. Dalichaouch, J.-S. Kang, M. S. Torikachvili, and M. A. Lopez de la Torre, Phys. Rev. Lett. **68**, 1034 (1992).

[5] K. R. Lea, M. J. M. Leask, and W. P. Wolf, J. Phys. Chem. Solids **23**, 1381 (1962).

[6] T. Tayama, T. Sakakibara, K. Kitami, M. Yokoyama, K. Tenya, H. Amitsuka, D. Aoki, Y. Ōnuki, and Z. Kletowski, J. Phys. Soc. Jpn. **70**, 248 (2001).

[7] E. Bucher, K. Andres, A. C. Gossard, and J. P. Maita, in *Low Temperature Physics LT-13*, edited by K. D. Timmerhaus, W. J. O'Sullivan, and E. F. Hammel, Vol. 2 (Springer, Berlin, 1974), pp. 322–326.

[8] T. Kawae, K. Kinoshita, Y. Nakaie, N. Tateiwa, K. Takeda, H. S. Suzuki, and T. Kitai, Phys. Rev. Lett. **96**, 027210 (2006).

[9] M. B. Maple, P.-C. Ho, V. S. Zapf, N. A. Frederick, E. D. Bauer, W. M. Yuhasz, F. M. Woodward, and J. W. Lynn, J. Phys. Soc. Jpn. **71**, 23 (2002).

[10] E. D. Bauer, N. A. Frederick, P.-C. Ho, V. S. Zapf, and M. B. Maple, Phys. Rev. B **65**, 100506 (2002).

[11] M. B. Maple, Z. Henkie, W. M. Yuhasz, P.-C. Ho, T. Yanagisawa, T. A. Sayles, N. P. Butch, J. R. Jeffries, and A. Pietraszko, J. Magn. Magn. Mater. **310**, 182 (2007).

[12] M. Kohgi, K. Iwasa, M. Nakajima, N. Metoki, S. Araki, N. Bernhoeft, J.-M. Mignot, A. Gukasov, H. Sato, Y. Aoki, and H. Sugawara, J. Phys. Soc. Jpn. **72**, 1002 (2003).

[13] H. Sugawara, S. Osaki, S. R. Saha, Y. Aoki, H. Sato, Y. Inada, H. Shishido, R. Settai, Y. Ōnuki, H. Harima, and K. Oikawa, Phys. Rev. B **66**, 220504 (2002).

[14] K. Kuwahara, K. Iwasa, M. Kohgi, K. Kaneko, N. Metoki, S. Raymond, M.-A. Méasson, J. Flouquet, H. Sugawara, Y. Aoki, and H. Sato, Phys. Rev. Lett. **95**, 107003 (2005).

[15] M. Yogi, T. Nagai, Y. Imamura, H. Mukuda, Y. Kitaoka, D. Kikuchi, H. Sugawara, Y. Aoki, H. Sato, and H. Harima, J. Phys. Soc. Jpn. **75**, 124702 (2006).

[16] Y. Aoki, T. Namiki, S. Ohsaki, S. R. Saha, H. Sugawara, and H. Sato, J. Phys. Soc. Jpn. **71**, 2098 (2002).

[17] T. Onimaru, K. T. Matsumoto, Y. F. Inoue, K. Umeo, Y. Saiga, Y. Matsushita, R. Tamura, K. Nashimoto, I. Ishii, T. Suzuki, and T. Takabatake, J. Phys. Soc. Jpn. **79**, 033704 (2010).

[18] T. Onimaru, N. Nagasawa, K. T. Matsumoto, K. Wakiya, K. Umeo, S. Kittaka, T. Sakakibara, Y. Matsushita, and T. Takabatake, Phys. Rev. B **86**, 184426 (2012).

[19] K. Iwasa, H. Kobayashi, T. Onimaru, K. T. Matsumoto, N. Nagasawa, T. Takabatake, S. Ohira-Kawamura, T. Kikuchi, Y. Inamura, and K. Nakajima, J. Phys. Soc. Jpn. **82**, 043707 (2013).

[20] I. Ishii, H. Muneshige, S. Kamikawa, T. K. Fujita, T. Onimaru, N. Nagasawa, T. Takabatake, T. Suzuki, G. Ano, M. Akatsu, T. Takabatake, and T. Suzuki, Phys. Rev. B **87**, 205106 (2013).

[21] A. Sakai and S. Nakatsuji, J. Phys. Soc. Jpn. **80**, 063701 (2011).

[22] A. Sakai, K. Kuga, and S. Nakatsuji, J. Phys. Soc. Jpn. **81**, 083702 (2012).

[23] T. J. Sato, S. Ibuka, Y. Nambu, T. Yamazaki, T. Hong, A. Sakai, and S. Nakatsuji, Phys. Rev. B **86**, 184419 (2012).

[24] K. Matsubayashi, T. Tanaka, A. Sakai, S. Nakatsuji, Y. Kubo, and Y. Uwatoko, Phys. Rev. Lett. **109**, 187004 (2012).

[25] R. Higashinaka, A. Nakama, M. Ando, M. Watanabe, Y. Aoki, and H. Sato, J. Phys. Soc. Jpn. **80**, SA048 (2011).

[26] I. Ishii, H. Muneshige, Y. Suetomi, T. K. Fujita, T. Onimaru, K. T. Matsumoto, T. Takabatake, K. Araki, M. Akatsu, Y. Nemoto, T. Goto, and T. Suzuki, J. Phys. Soc. Jpn. **80**, 093601 (2011).

[27] V. W. Burnett, D. Yazici, B. D. White, N. R. Dilley, A. J. Friedman, B. Brandom, and M. B. Maple, J. Solid State Chem. **215**, 114 (2014).

[28] D. Yazici, B. D. White, P.-C. Ho, N. Kanchanavatee, K. Huang, A. J. Friedman, A. S. Wong, V. W. Burnett, N. R. Dilley, and M. B. Maple, Phys. Rev. B **90**, 144406 (2014).

[29] A. C. Larson and R. B. Von Dreele, General structure analysis system (GSAS), Los Alamos National Laboratory Report LAUR 86-748 (2004).

[30] B. H. Toby, J. Appl. Crystallogr. **34**, 210 (2001).

[31] K. Iwasa, Y. Watanabe, K. Kuwahara, M. Kohgi, H. Sugawara, T. Matsuda, Y. Aoki, and H. Sato, Phys. B (Amsterdam) **312**, 834 (2002).

[32] M. B. Maple, Phys. B (Amsterdam) **215**, 110 (1995).

[33] M. B. Maple, M. C. de Andrade, J. Herrmann, Y. Dalichaouch, D. A. Gajewski, C. L. Seaman, R. Chau, R. Movshovich, M. C. Aronson, and R. Osborn, J. Low Temp. Phys. **99**, 223 (1995).

[34] J.-H. Chung, M. Matsuda, S.-H. Lee, K. Kakurai, H. Ueda, T. J. Sato, H. Takagi, K.-P. Hong, and S. Park, Phys. Rev. Lett. **95**, 247204 (2005).

[35] N. A. Frederick and M. B. Maple, J. Phys.: Condens. Matter **15**, 4789 (2003).